

AWARD NUMBER: 01HQGR0049

Recipient: University of California, Santa Barbara/Institute for Crustal Studies

Principal Investigator: Daniel Lavallée, Ralph Archuleta and Peng-Cheng Liu

MODELING AND ESTIMATES OF NONLINEAR EFFECTS IN STRONG EARTHQUAKE
MOTION FOR THE LOS ANGELES AREA

Program Element II: Research on Earthquake Occurrence and Effects.

Research supported by the U.S. Geological Survey (USGS), Department of the Interior, under USGS award number 01HQGR0049. The views and conclusions contained in this document are those of the authors and should not be interpreted as necessarily representing the official policies, either expressed or implied, of the U.S. Government.

Award number: 01HQGR0049

MODELING AND ESTIMATES OF NONLINEAR EFFECTS IN STRONG EARTHQUAKE MOTION FOR THE LOS ANGELES AREA

Daniel Lavallée, Ralph Archuleta and Peng-Cheng Liu
Institute for Crustal Studies,
University of California, Santa Barbara,
Santa Barbara, CA 93106

Telephone numbers: 805-893-8446 (Lavallée); 805-893-8441 (Archuleta); 805-893-8446 (Liu)

Fax number: 805-893-8649

E-mail addresses: daniel@crustal.ucsb.edu; ralph@crustal.ucsb.edu; pcliu@crustal.ucsb.edu

TECHNICAL ABSTRACT

In this project, we have pursued the development and validation of a robust and simple model of nonlinear soil dynamics to study seismic wave propagation. The nonlinear soil model used in this study includes effects such as anelasticity, hysteretic behavior and cyclic degradation due to pore water pressure. Strong motion data recorded during the 17 January 1994 Northridge earthquake have been used to validate the nonlinear soil model. Signals recorded at several sites are good candidates to investigate nonlinear effects. Four sites have been selected for this project: the Jensen Generator Building (JMB or JFP), the Newhall Fire Station (NWH) site, the Rinaldi (RIN) site and the Knoll Elementary School (KES or SMI). For each site, measurement of ground motion observed at the near-by bedrock site has been coupled with the nonlinear model to generate scenarios of ground shaking. Two situations have been investigated: one that includes the effect of pore pressure (effective stress analysis) and the second without it (total stress analysis). In the first case, the nonlinear model propagated a signal through layers of saturated material; whereas only layers of dry materials are used in the second case. Many scenarios of nonlinear ground shaking have been computed. Using trial-and-error modeling and comparison with the observed time history, we were able to refine the synthetic accelerograms.

The results of the numerical experiments conducted at these sites support the assumption that a nonlinear effect contributes significantly to the ground shaking observed at the surface of three of the four sites under study.

- The numerical predictions of the nonlinear soil model for the JMB site are in very good agreement with the recorded motion.
- Pore pressure cyclic mobility contributes significantly to the ground shaking observed at the surface of the JMB and the SMI sites.
- Depletion of the high frequency in the signal is in good agreement with both the recorded and synthetic accelerations of the JMB and the SMI sites.
- Although nonlinear effects took place at NWH site, it is not clear that pore pressure plays a significant part in the recorded motion.
- The numerical results for the RIN site are inconclusive.

We have to stress that in this study, conclusive finding of nonlinearity is based on direct simulations of nonlinear soil dynamics and the quantification of the nonlinearity in terms of the model parameters. According to this, nonlinear soil dynamics provides a satisfactory model to explain and predict behavior observed at three of the four the sites used in this study.

MODELING AND ESTIMATES OF NONLINEAR EFFECTS IN STRONG EARTHQUAKE
MOTION FOR THE LOS ANGELES AREA

Award number: 01HQGR0049

Daniel Lavallée, Ralph Archuleta and Peng-Cheng Liu
Institute for Crustal Studies,
University of California, Santa Barbara,
Santa Barbara, CA 93106

Telephone numbers: 805-893-8446 (Lavallée); 805-893-8441 (Archuleta); 805-893-8446 (Liu)

Fax number: 805-893-8649

E-mail addresses: daniel@crustal.ucsb.edu; ralph@crustal.ucsb.edu; pcliu@crustal.ucsb.edu

Program Element II: Research on Earthquake Occurrence and Effects.

Key words: Wave Propagation, Strong ground motion

NON-TECHNICAL ABSTRACT

We have pursued the development and validation of the nonlinear model of soil dynamics using U.S. Geological Survey sponsored studies and strong motion data recorded during the 17 January 1994 Northridge earthquake (with a magnitude 6.7). Four sites have been selected for this project. Modeling of ground motions at these four sites confirm the presence of nonlinear effects in the signal observed at the JMB, the NWH and the SMI sites. Since the ground shaking at sediment (nonlinear) sites is different from the shaking at rock (linear) site, prediction of nonlinear effects is essential to manage and mitigate earthquake hazards.

PROJECT DESCRIPTION AND RESULTS

1 INTRODUCTION

We have pursued the development and validation of the nonlinear model of soil dynamics using U.S. Geological Survey sponsored studies and strong motion data recorded during the 17 January 1994 Northridge earthquake (M_w 6.7). The data available included borehole velocity profiles, weak to strong motion records, and dynamic soil laboratory tests. Several sedimentary stations have responded with sharp resonance peaks (Field *et al.*, 1996; Archuleta *et al.*, 1998; and Cultrera *et al.*, 1998). Signals recorded at these sites are good candidates to investigate nonlinear effects. Four sites have been selected for this project: the Jensen Generator Building (JMB or JFP), the Newhall Fire Station (NWH) site, the Rinaldi (RIN) site and the Knoll Elementary School (KES or SMI).

The formulation of the soil model includes nonlinear effects such as anelasticity, hysteretic behavior, and cyclic degradation due to pore water pressure. The hysteresis model used is the generalized Masing rules (Archuleta *et al.*, 1999; 2000; Bonilla, 2000; and Lavallée *et al.*, 2002). The effect of pore pressure has been incorporated using a model developed by Towhata and Ishihara, 1985; and Iai, 1990a, b. The nonlinear soil model and its implementation are discussed at length in Section 2.

There are essentially three ways to validate a numerical model. The first one is the comparison with analytical solutions for simple situations. Due to the complexity of the formulation of the hysteresis and the pore pressure models, it was not possible to implement this procedure. Another method of validation, consists in the comparison of the numerical solutions obtained by different models (see Archuleta *et al.*, 2002 for a comparison of ground motions generated by nonlinear soil model, including the one discussed in Section 2). Finally the model can be validated using seismic observations. The results of this validations using strong motion data recorded during the 17 January 1994 Northridge earthquake are presented in Section 3.

2 THE NONLINEAR SOIL MODEL

A. Theoretical foundation of the model

The propagation of seismic waves directly depends on the mechanical properties of the material. In a typical geological setting, the shear-wave velocity of the sediments increases with depth. Consequently, seismic wave paths are bent toward the earth surface, and hit the surface with almost normal incidence. Empirical results also show that the shear wave dominates the seismic signal. Thus, in a first approximation, the wave propagation can be reduced to a one-dimensional shear wave. The model assumes continuum mechanics and implements a computer-based numerical integration of the one-dimensional shear wave equation of motion with appropriate boundary and initial conditions:

$$\rho \frac{\partial^2 u}{\partial t^2} = \frac{\partial \tau}{\partial z} \quad (1)$$

Here $u(z,t)$ denotes the displacement field perpendicular to the vertical axis at position z and time t , ρ is the unstrained density of the material, and $\tau(z,t)$ is the shear stress.

To study and understand the phenomenology of nonlinear soil response to earthquake, we have developed a numerical model that captures the essential physics of nonlinearity in soil. The nonlinear effects included anelasticity, hysteretic behavior and cyclic degradation due to pore water pressure.

Anelasticity describes through a constitutive equation the stress-strain relationship in terms of the soil parameters. A simple example is the hyperbolic model given by the following equation:

$$\tau = G_{\max} \gamma \quad G(\gamma) = \frac{G_{\max} \gamma}{1 + \left(\frac{\gamma}{\gamma_{\max}} \right)^2} \quad (2)$$

where $G(\gamma)$ is the strain-dependent shear modulus, $\gamma(z, t) = \partial u(z, t) / \partial z$ denotes the shear strain. The parameter G_{max} is the maximum shear modulus at low strain, σ_{max} is the maximum stress that the material can support in the initial state. (Note that although we only consider the case where the stress is a function of the strain, the procedure outlined below remains valid for the situation where the strain is a function of the stress.)

The second effect, hysteresis, describes the behavior of the stress strain relationship under cyclic or noncyclic loading. In this project, we developed a new hysteresis model, the generalized Masing rule (Archuleta *et al.*, 1999, 2000; Bonilla, 2000; and Lavallée *et al.*, 2002).

B Introduction to the generalized Masing rules

Hysteresis behavior can be implemented with the help of the Masing and extended Masing rules (see Kramer, 1996). The basic idea in the Masing formulation is that the functional behavior governing the relation between the stress and the strain for the first loading path in stress-strain space will also govern the subsequent unloading and reloading paths. Given the relation for the first loading path

$$\sigma = F_{bb}(\gamma) \quad (3)$$

where $F_{bb}(\gamma)$ is called the backbone or skeleton curve, the subsequent unloading and reloading paths are essentially a translation and dilatation of the backbone curve given by the following relation

$$\frac{\sigma - \sigma_f}{c_H} = F_{bb} \left(\frac{\gamma - \gamma_f}{c_H} \right) \quad (4)$$

The translation is given with respect to the coordinate (γ_f, σ_f) , the strain and the stress at the turning point, respectively. A turning point is defined by the condition $d\sigma(t)/dt = 0$. In Masing's original formulation, the dilatation was given by a hysteresis scale factor c_H equal to 2.0. However, these rules are inadequate to describe the hysteretic behavior of material under noncyclic loadings (see Pyke, 1979 and references therein; also Li and Liao, 1993). For instance, numerical simulations with noncyclic signals suggest that application of the Masing rules leads to an unphysical situation—such as the computed stress exceeding the strength of the material.

A first extension to the Masing rules was obtained by releasing the constraint $c_H = 2$ (Bonilla *et al.*, 1998; and Lavallée *et al.*, 2002). As part of our investigation we show that using $c_H \neq 2$ provides a better fit to a sand sample under a cyclic loading condition. The Masing rules are further generalized by allowing c_H to take different values after each turning point.

In the generalized Masing rules, the value of the hysteresis scale factor $c_H^{(n)}$ is related to the physical properties of the material and to one free parameter γ_f —the value of the strain at the point where the loading/unloading branch intersects the backbone curve. In the stress-strain space, each unloading, or reloading, follows a path that converges to the fiducial point given by $[\gamma_f, F_{bb}(\gamma_f)]$, or $[\gamma_f, F_{bb}(\gamma_f)]$. The parameter $c_H^{(n)}$ is the hysteresis scale factor after the n^{th} turning point with $n \geq 1$ ($n = 0$ corresponds to the first loading with $\sigma(\gamma)$ given by the backbone curve). The hysteresis scale factor controls the curvature of each unloading, or reloading accordingly. The value of $c_H^{(n)}$ is modified at every n^{th} turning point to take into account its previous value. Hence, $[\gamma_f, F_{bb}(\gamma_f)]$ can be seen as the focusing point of the reloading paths, and $[\gamma_f, F_{bb}(\gamma_f)]$ as the focusing point of the unloading paths.

A third rule is supplemented to deal with the behavior of the stress-strain path when the strain values exceed the critical value γ_f (Archuleta *et al.*, 1999; and Lavallée *et al.*, 2002). The third rule is needed when $|\gamma^{(1)}| < |\gamma_f|$ and optional when $|\gamma_f| = |\gamma^{(1)}|$ or $|\gamma_f| \geq |\gamma^{(1)}|$ (where $\gamma^{(1)}$ is the strain at the first turning point). The third rule specifies that when the strain absolute values exceeds

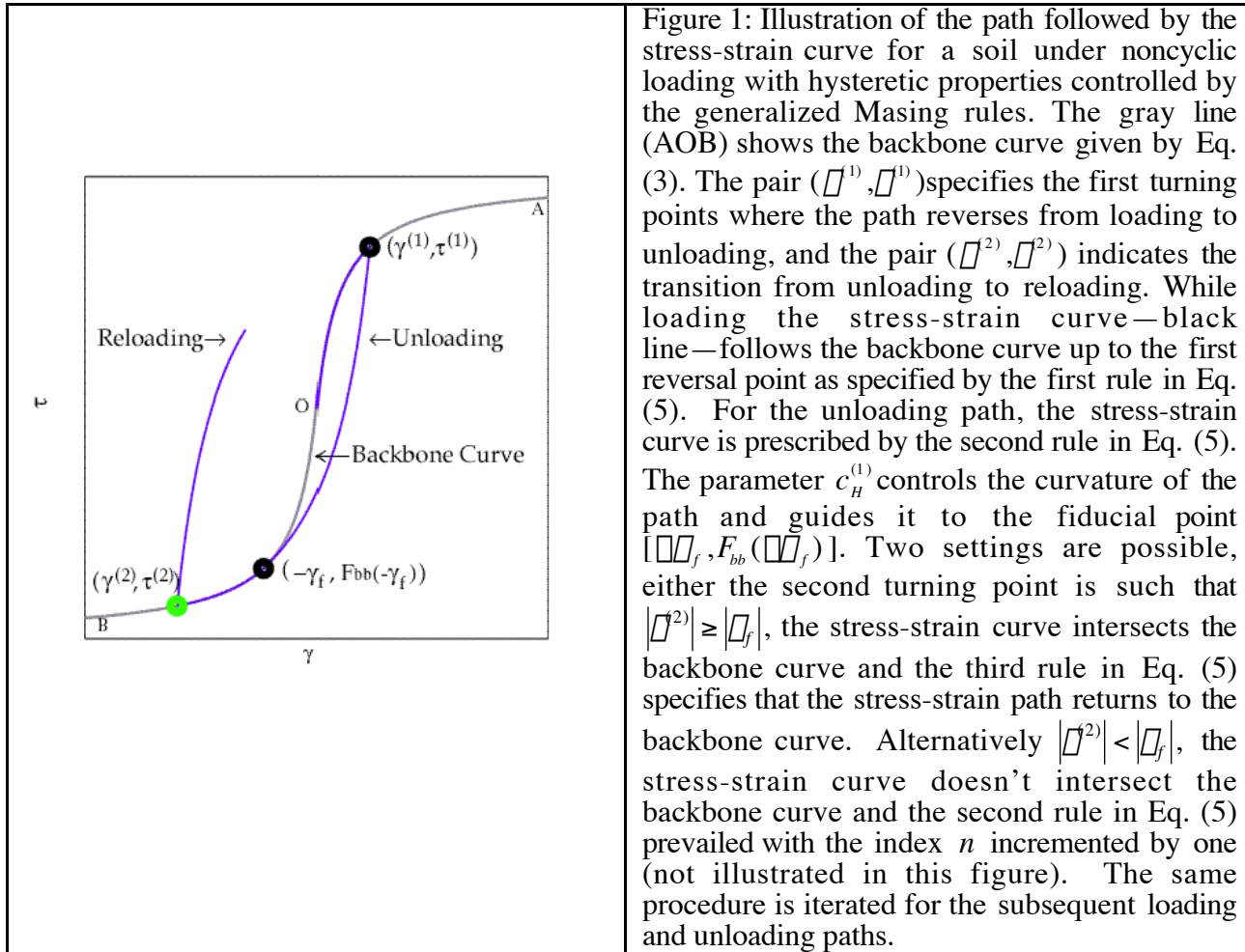
\square_f , the unloading or reloading curve follows the backbone curve until the next reversal point. The generalized Masing rules can be written:

$$\begin{aligned} \square(\square) = & \begin{array}{c} \square \\ \square \\ \square \\ \square \\ \square \\ \square \\ \square \end{array} \begin{array}{c} F_{bb}(\square) \\ c_H^{(n)} F_{bb} \frac{\square \square \square^{(n)}}{c_H^{(n)}} + \square^{(n)} \\ F_{bb} \left(\text{Sign} \left(\frac{d\square}{dt} \right) \square \right) \end{array} \begin{array}{l} \square < \square^{(1)}, n = 0 \\ |\square \square | \square_f|, n \geq 1 \\ |\square| \geq |\square_f|, n = 0 \end{array} \quad (5) \end{aligned}$$

$\bar{\sigma}^{(n)}$ and $\bar{\epsilon}^{(n)}$ are the stress and the strain at the n^{th} turning point, where $\bar{\epsilon}^{(n)}$ is given by the following relation:

$$\square^n = \prod_{i=2}^n c_H^{(i \square 1)} F_{bb} \left(\frac{\square^{(i)} \square^{(\square 1)}}{c_H^{(i \square 1)}} \right) + F_{bb}(\square^{(1)}) \quad (6)$$

The time derivative in Eq. (5) is estimated at any time between the n^{th} and the $(n + 1)^{th}$ turning point. A schematic illustration of the generalized Masing rules is presented in Figure 1. A comparison of the behavior of the strain and stress curves is shown in Figure 2 using both the generalized and the original Masing rules.



Using Eq. (2), the expression for $c_H^{(n)}$ can be estimated

$$c_H^{(n)} = \frac{\left(F_{bb} \left(\text{Sign} \left(\frac{d\bar{\epsilon}}{dt} \right) \right) \bar{\epsilon}_f \right) \left| \bar{\epsilon}_f \right| \left| \bar{\epsilon}^{(n)} \right| \text{Sign} \left(\frac{d\bar{\epsilon}}{dt} \right) \left| \bar{\epsilon}_f \right| \left| \bar{\epsilon}^{(n)} \right|}{\left(\text{Sign} \left(\frac{d\bar{\epsilon}}{dt} \right) \right) \left| \bar{\epsilon}_f \right| \left| \bar{\epsilon}^{(n)} \right| \bar{\epsilon}_{\max} + \left(\bar{\epsilon}^{(n)} \right) \bar{\epsilon} F_{bb} \left(\text{Sign} \left(\frac{d\bar{\epsilon}}{dt} \right) \right) \left| \bar{\epsilon}_f \right| \left| \bar{\epsilon}^{(n)} \right| \bar{\epsilon}_{\text{ref}}} \quad (7)$$

for the hyperbolic model with a reference strain $\bar{\epsilon}_{\text{ref}} = \bar{\epsilon}_{\max} / G_{\max}$. This expression of $c_H^{(n)}$ reduces to other hysteretic models for special values of $\bar{\epsilon}_f$. When $\bar{\epsilon}_f = 0$, the relation for $c_H^{(n)}$ corresponds to the Cundall-Pyke hypothesis (Pyke, 1979) for all n . When $\bar{\epsilon}_f = \bar{\epsilon}^{(1)}$ and $\bar{\epsilon}(t)$ is a periodical function of time, the expression for $c_H^{(n)}$ is the constant 2 for all n and therefore corresponds to the original formulation of the Masing rules.

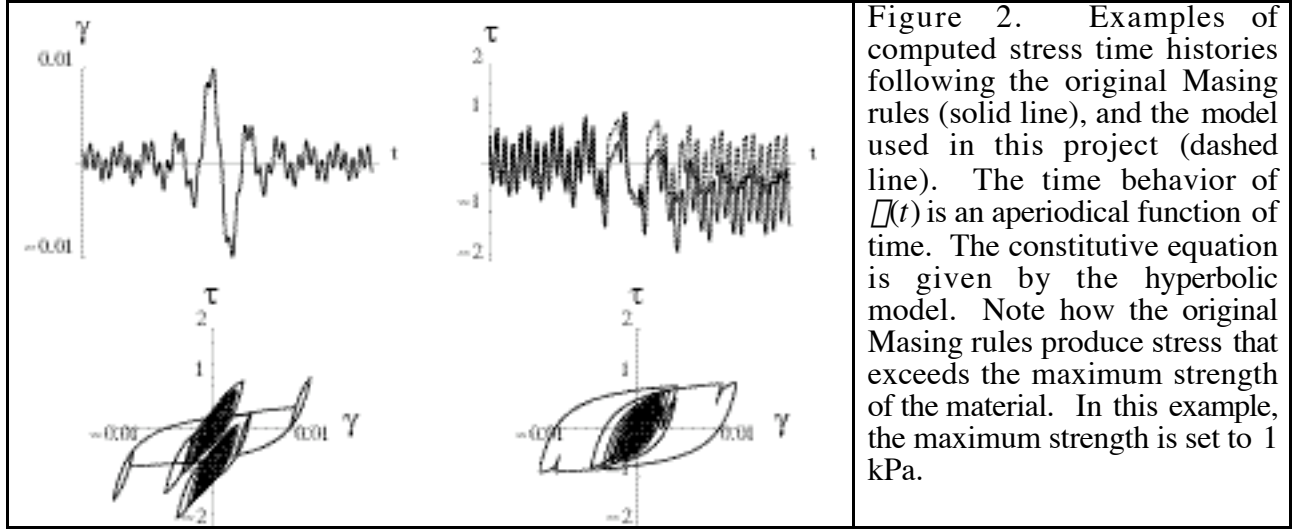


Figure 2. Examples of computed stress time histories following the original Masing rules (solid line), and the model used in this project (dashed line). The time behavior of $\bar{\epsilon}(t)$ is an aperiodical function of time. The constitutive equation is given by the hyperbolic model. Note how the original Masing rules produce stress that exceeds the maximum strength of the material. In this example, the maximum strength is set to 1 kPa.

In the simplest implementation of the generalized Masing rule $\left| \bar{\epsilon}_f \right| = \left| \bar{\epsilon}^{(1)} \right|$, and no other rules are needed to maintain the stress values between $\pm \bar{\epsilon}_{\max}$. Note that this case is even simpler than the Masing and extended Masing formulation that requires a total of four rules (Kramer, 1996). The synthetic accelerograms presented below used this value of $\bar{\epsilon}_f$ with the optional third rule of Eq. (6) also contained in the hysteresis model. Using trial and error modeling, we have found that this choice optimizes the agreement between the synthetic and observed accelerograms. Both beside simplicity, there is no physical or mathematical reason to confine $\bar{\epsilon}_f$ to this value. Other choices are discussed and illustrated in Bonilla (2000) and Lavallée *et al.*, (2002).

C The effect of pore pressure

In several major seismic events, such as the 1995 Hyogo-ken Nambu (Kobe) earthquake, the loss of soil cohesion and the subsequent damage to structure are attributed to liquefaction (Seed 1966; an Ishihara 1985; and Bardet *et al.* 1995). Observations of the spikes late in the acceleration time history has been also attributed to pore pressure effect (see Archuleta, 1998). To reproduce these events require the addition of pore pressure to the numerical model describe in Sections 2A and 2B. The effect of pore pressure has been incorporated using a model developed by Towhata and Ishihara, 1985; Iai, 1990a, b. (Details of the implementation of pore pressure is also discussed in Archuleta *et al.*, 1999.) The constitutive equation corresponds to a plane strain multiple mechanism model—or multi inelastic spring model—used to simulate cyclic mobility of sands under undrained conditions. In this model, the pore pressure development is correlated to the shear work.

D Numerical implementation of the nonlinear soil model

Finally we have developed a code to compute seismic wave propagation throughout nonlinear geomaterial. The numerical integration of the wave equation (Eq. 1) is performed using a velocity-displacement-stress staggered grid second order finite difference formulation (Mozco, 1998). The boundary conditions correspond to traction free conditions at surface. Rigid and elastic boundary conditions can be specified at the soil-rock interface (Joyner and Chen 1975). The nonlinear code is called NOAH. A detailed discussion of the code can be found in Bonilla (2000).

In summary the nonlinear soil model used the following parameters. The properties of the soil model are characterized by the following parameters: the shear wave velocity v_s , the p-wave velocity v_p , the density ρ , the coefficient of earth at rest K_0 , the angle of internal friction ϕ . These parameters are used to compute G_{max} and μ_{max} in Eq. (2). Friction is included by the implementation of the quality factor Q (a viscosity coefficient η is also included by adding the term $\eta \partial \epsilon / \partial t$ to the right hand side of Eq. (2) but only to insure numerical stability of the code). The maximum damping value at large stress H_{max} is also included. (This last parameter has been introduced lately in the model to achieve a better description of the hysteresis damping—see Lavallée *et al.*, 2002 for details). Six additional parameters are needed to describe the pore pressure buildup: the transformation phase angle ϕ_p , the parameters p_2 , p_2 and w_1 that are related to the excess pore water pressure generation, and the parameters c_1 and S_1 .

3 MODELING OF NONLINEAR STRONG MOTION DURING THE 1994 NORTHRIDGE EARTHQUAKE

A Description of the procedure and of the sedimentary sites

To validate the nonlinear soil model described in the Section 2, we have designed numerical experiment using near-source-free field acceleration time histories recorded in the 1994 Northridge earthquake. The 17 January 1994 Northridge earthquake (M_w 6.7) has greatly increased the available set of strong ground motion records for the Los Angeles area. According to several authors—Field *et al.* (1996), Archuleta *et al.* (1998); and Cultrera *et al.*, (1998)—these records include interesting manifestations of nonlinearity at certain sedimentary sites. Furthermore, the velocity profiles of four of these sedimentary sites (JFP, NWH, RIN and SMI) have been measured either by the ROSRINE project or by the U.S. Geological Survey (Gibbs *et al.*, 1996, 1999, 2000). Signals recorded at these sites are good candidates to validate the nonlinear soil model described in Section 2.

Each of the sediment sites—JFP, NWH, RIN and SMI—has been matched to a near-by reference site corresponding to hard rock—JGB, PCD, LAD and ETEC, respectively. Hard rock sites are characterized by the higher shear velocity speeds. Signals recorded at these sites are presumed to be free of nonlinear effects (at least for the frequency band relevant for this study). The velocity profiles of the hard rock sites have been measured either by the ROSRINE project or by the U.S. Geological Survey (Gibbs *et al.*, 1996, 1999, 2000).

The following procedure was used to compute synthetic accelerograms at each sedimentary stations. The measured velocity profile is used to deconvolve the signal recorded at the hard rock site to approximate the input motion at the rock base level. The soil at the sedimentary site is approximated by a stack of horizontal uniform layers; each layer is characterized by a set of parameters. The nonlinear soil dynamic model discussed in Section 2 is used to propagate the input signal following the geotechnical descriptions of the ROSRINE and USGS velocity models. Two situations have been investigated, one that includes the effect of pore pressure (effective stress analysis) and the second without it (total stress analysis). In the first case, the nonlinear model is used to propagate a signal through layers of saturated material, whereas only layers of dry materials are used in the second case. Unfortunately information about most of the model parameters listed in the previous section is not available; only the measured values of the shear wave velocity v_s , and the P-wave velocity v_p are available. This difficulty can be palliated by computing many scenarios of

the ground shaking at the surface for different range of parameter values. For each sedimentary site, many scenarios of nonlinear ground shaking have been computed. All the accelerograms were computed up to a maximum frequency of 10 Hz. For each accelerogram, the peak ground accelerations has been estimated and spectral analysis of the synthetics and recorded surface motions have been computed. Using trial-and-error modeling and comparison with the observed time history, we were able to refine the synthetic accelerograms. Each of the recorded components have been rotated into fault normal (210°) and fault parallel (120°). We report the results for the horizontal component (120°) and (210°) of the JFP, NWH, RIN and SMI sites.

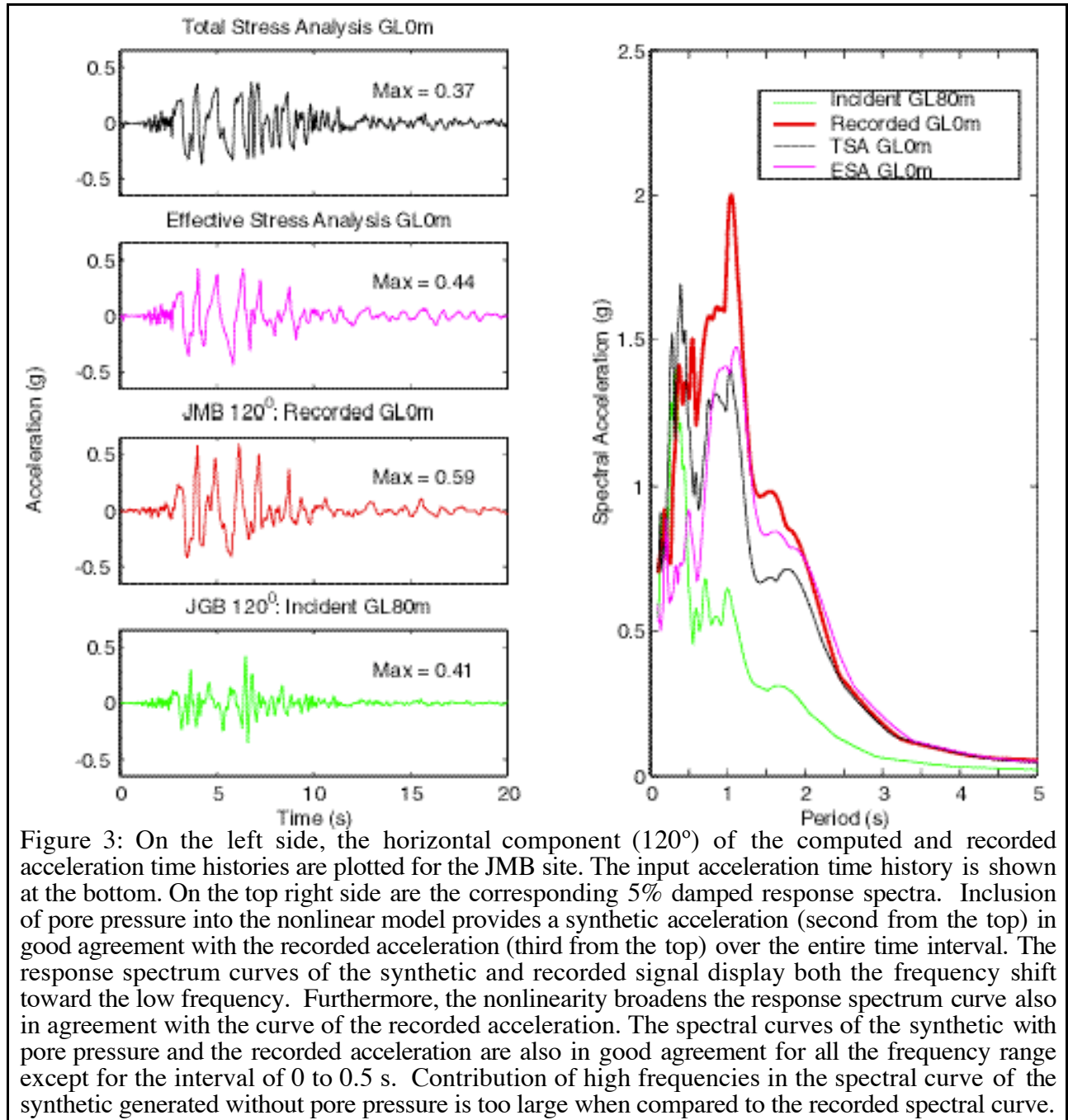
B The JFP site

The results of the numerical experiments conducted with this site support the assumption that pore pressure cyclic mobility did contribute significantly to the ground shaking observed at the surface. The geotechnical parameters are summarized in Table 1. The surface waveforms and their respective response spectra are illustrated in Figures 3 and 4.

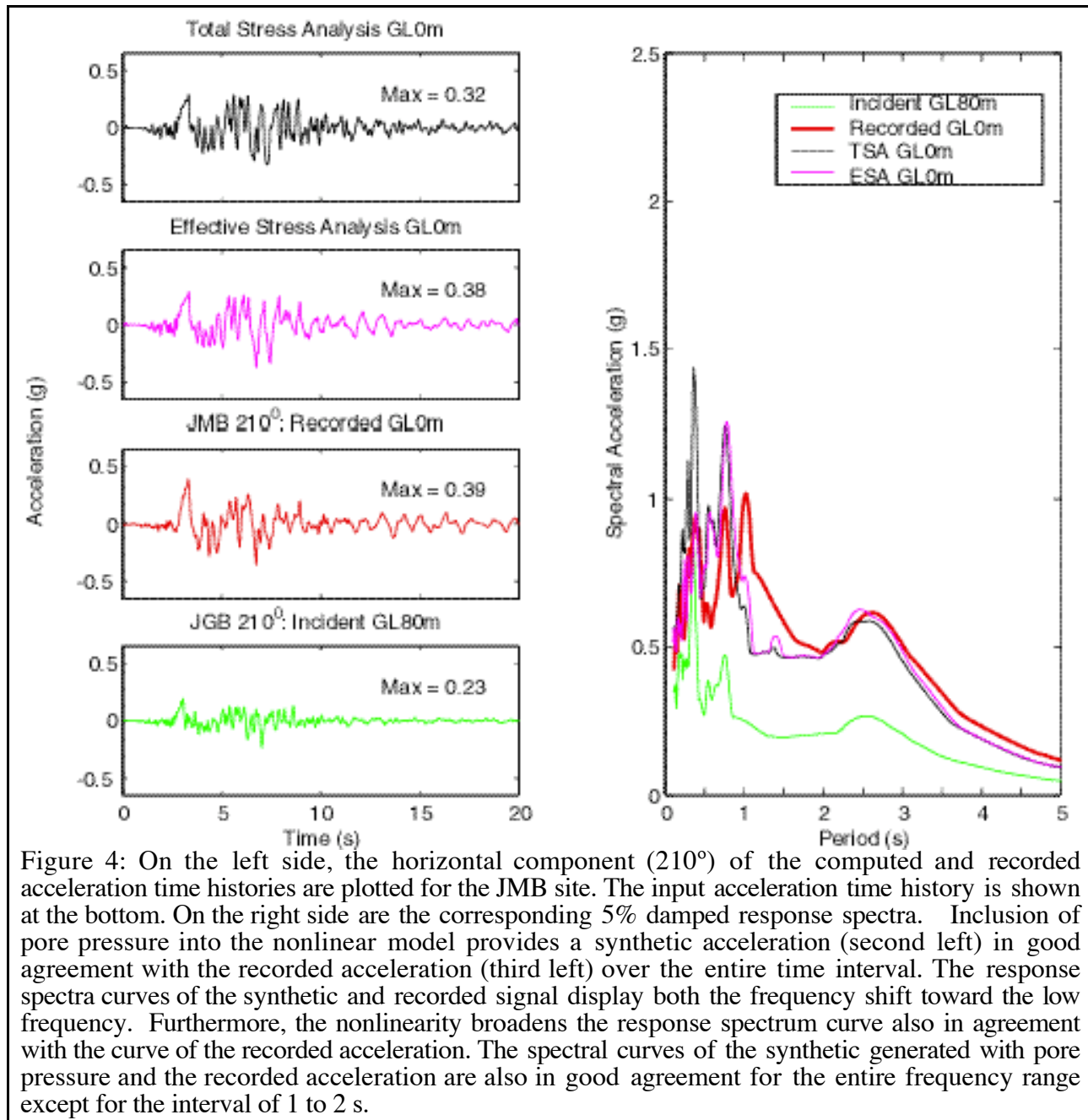
Table 1: Parameters for the nonlinear modeling at the: the parameter v_s is the shear wave velocity, v_p the p-wave velocity, and ρ the density, and Q the quality factor. For all layers, the coefficient of earth at rest is given by $K_0=1.$, the angle of internal friction $\phi=35^\circ$, the viscosity coefficient $\eta=5 \times 10^{15}$, and $H_{\max}=30\%$. The layers are numbered from 1 to 6. The water table is located at 9 m depth. The last layer BR, includes the information at the bedrock level. Only layer 2 is capable of building up pore pressure.

| LAYER NO. | DEPTH (M) | v_s (m/s) | v_p (m/s) | ρ (KG/M ³) | Q | PARAMETERS FOR DILATANCY | | | | | |
|-----------|-----------|-------------|-------------|-----------------------------|-----|--------------------------|-------|-------|-------|-------|-------|
| | | | | | | $\bar{\rho}_p$ | p_1 | p_2 | w_1 | c_1 | S_1 |
| 1 | 9 | 298 | 754 | 1800 | 20. | | | | | | |
| 2 | 15. | 256 | 522 | 1800 | 20. | 24.8 | 0.5 | 0.6 | 7. | 1 | .01 |
| 3 | 23 | 564. | 902 | 1900 | 20. | | | | | | |
| 4 | 35. | 556 | 2215 | 2000 | 20. | | | | | | |
| 5 | 63. | 556 | 1978 | 2000 | 20. | | | | | | |
| 6 | 80. | 684 | 2134 | 2000 | 20. | | | | | | |
| BR | | 684 | | 2000 | | | | | | | |

A characteristic feature of simulations including pore pressure effects for this site is the depletion of the high frequency in the signal in good agreement with the recorded acceleration. None of the scenarios, generated without pore pressure, were able to reproduce this feature.



Spiky waveforms in the tail can be detected in both synthetic and observed accelerograms as illustrated in Figure 4. Similar conclusions applied to the other horizontal component (210°) of the JMB site. Note also that it is possible to improve the fit between the observed and synthetics time histories for each component separately by using a different set of values for the model parameters for the two components. This suggests the presence of anisotropic effect in the soil sediment.



C The NWH site

For this site, the procedure described above has been slightly modified. The input motion was given by the surface accelerograms recorded at the PCD site. The data recorded by ROSRINE shows that the velocity profile of the PCD site near the surface (approximately 1300m/sec at GL-06) is higher than the velocity profile of the NWH site at bedrock level (approximately 850m/sec at GL-100). For this reason, the signal recorded at the surface of the PCD site provides a reasonable basis for approximating the incident base rock motion at the NWH site. Note that this procedure grants an extra degree of freedom in the location of the base rock motion. Numerical computation of surface motions from base rock motion located at different depths between GL-80 to GL-120 did not show any important modification in the amplitude or the phase. Also the results of the logging at the PCD site reported by ROSRINE do not include values of the velocity profile near the surface

(GL-0 to GL-5.5). We assumed a velocity profile similar to the one recorded between GL-5.5 and 8.5 and used this value for the base rock motion at the NWH site. The geotechnical parameters are summarized in Table 2. The surface waveforms and their respective response spectra are illustrated in Figures 5 and 6.

Table 2: For all layers, the coefficient of earth at rest is given by $K_0=1.$, the angle of internal friction $\varphi=40^\circ$, the viscosity coefficient $\eta=5 \times 10^{15}$, and $H_{\max}=30\%$. The layers are numbered from 1 to 7. The water table is located at 27 m depth. The last layer BR, includes the information at the bedrock level. Only layer 5 can experience pore pressure buildup.

| LAYER NO. | DEPTH (M) | v_s (m/s) | v_p (m/s) | ρ (KG/M ³) | Q | PARAMETERS FOR DILATANCY | | | | | |
|-----------|-----------|-------------|-------------|-----------------------------|-----|--------------------------|-------|-------|-------|-------|-------|
| | | | | | | φ_p | p_1 | p_2 | w_1 | c_1 | S_1 |
| 1 | 6 | 186.75 | 333.13 | 1800 | 20. | | | | | | |
| 2 | 12. | 230.04 | 457.74 | 1800 | 20. | | | | | | |
| 3 | 15.5 | 277.94 | 507.61 | 1800 | 20. | | | | | | |
| 4 | 27. | 308.06 | 637.65 | 1800 | 20. | | | | | | |
| 5 | 35. | 550.06 | 1151.7 | 1950 | 33. | 32° | 0.45 | 0.6 | 5 | 1 | 0.01 |
| 6 | 54. | 677.6 | 1371.4 | 2000 | 33. | | | | | | |
| 7 | 90. | 750.07 | 2036.9 | 2100 | 33. | | | | | | |
| BR | | 1300. | | 2300 | | | | | | | |

The results of the numerical experiments conducted at this site support the assumption that nonlinear effect contributed significantly to the ground shaking observed at the surface. However contrary to the results obtained for the JMB site, it is not clear that that pore pressure plays a significant part in the recorded accelerograms at the NWH site. For both components, the total stress modeling provides computed surface accelerations that reproduce fairly well the recorded motion. As before, the results could have been improved by relaxing the assumption that the soil is isotropic.

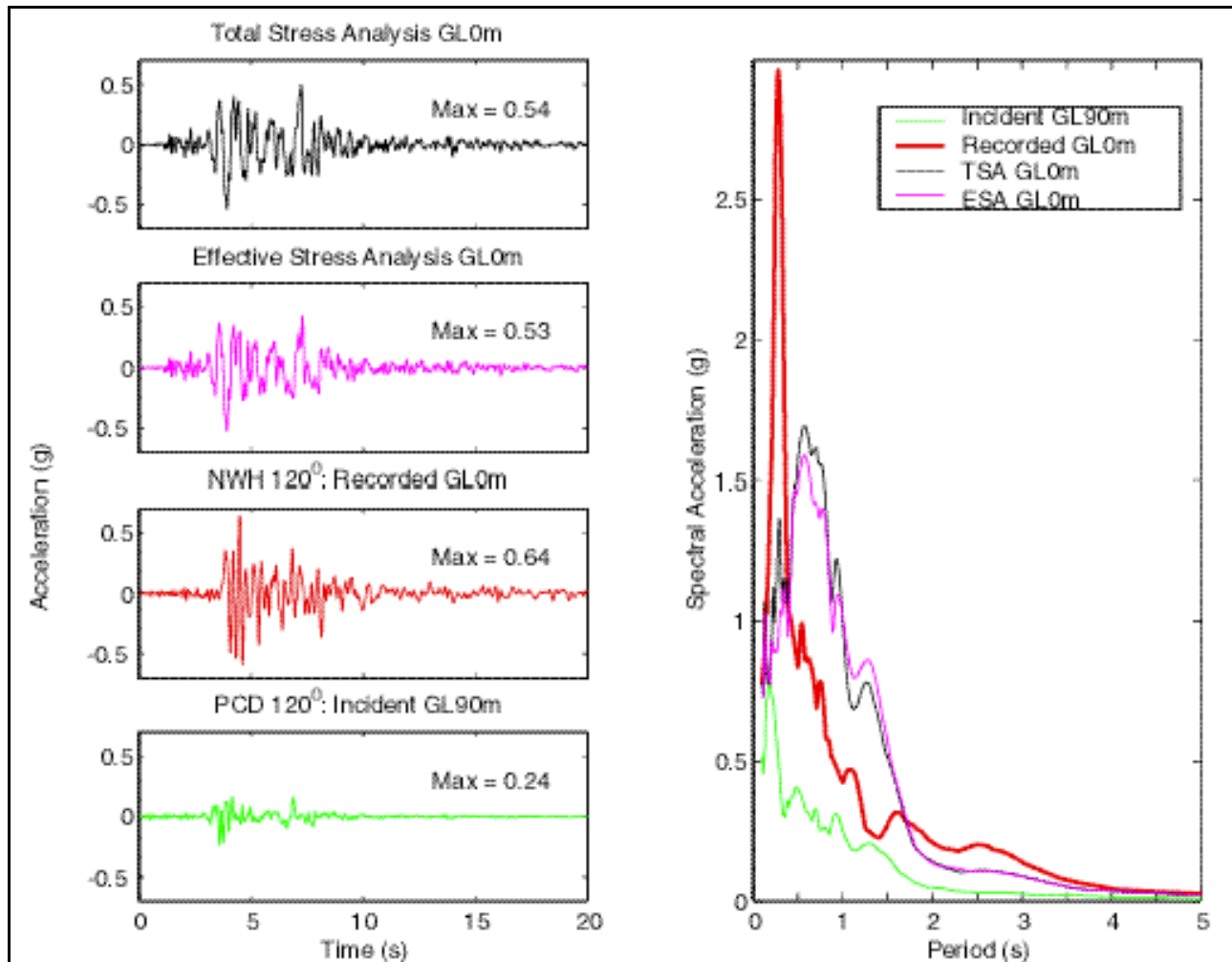
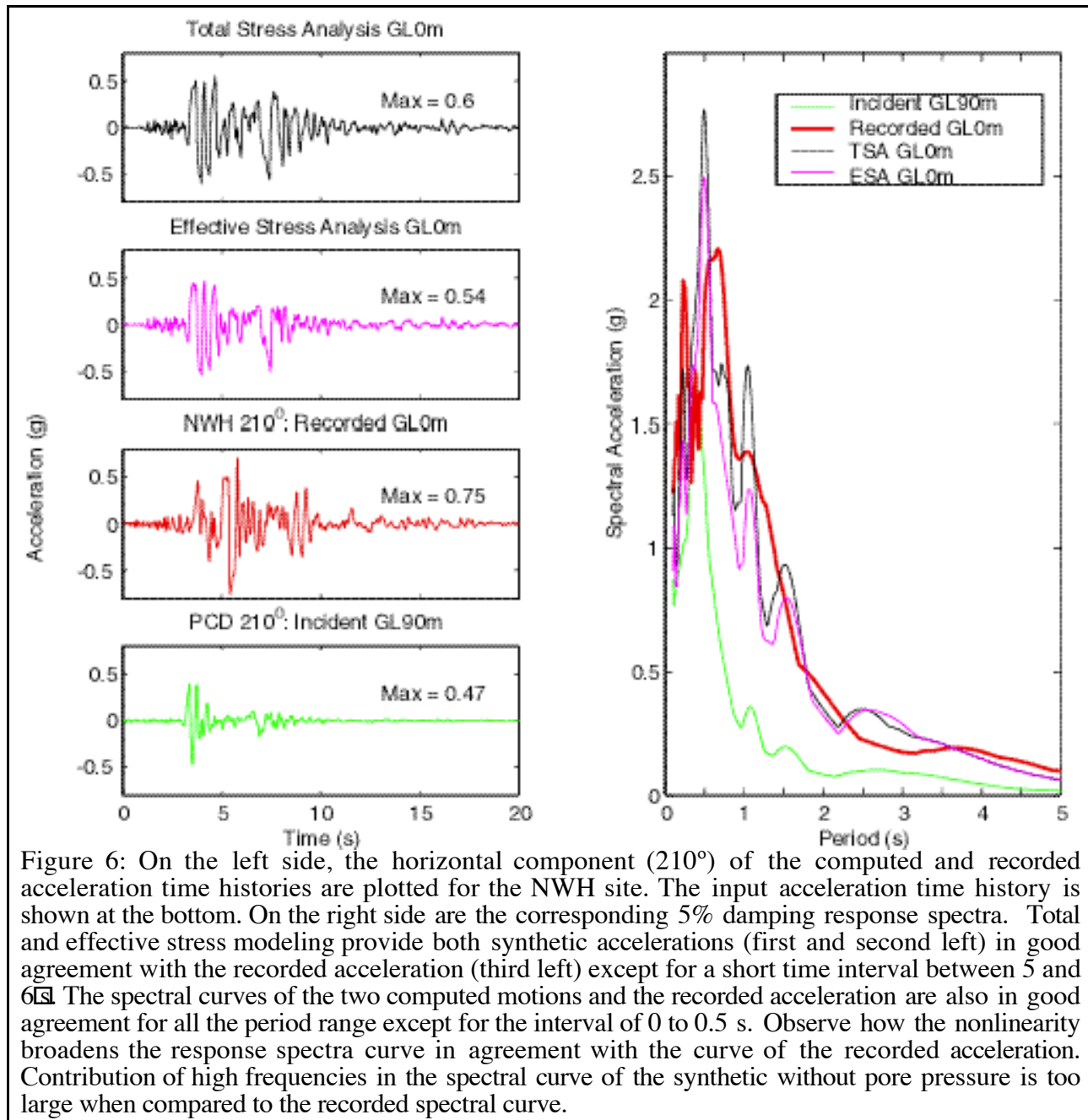


Figure 5: On the left side, the horizontal component (120°) of the computed and recorded acceleration time histories are plotted for the NWH site. The input acceleration time history is shown at the bottom. On the right side are the corresponding 5% damped response spectra. Total and effective stress modeling provide both synthetic accelerations (top and 2nd from the top) in good agreement with the recorded acceleration (3rd from the top) except for two short time intervals: first between 4 and 5 s; second between 6 and 7 s. However, the spectral curves of the two computed motions are too high when compared to the recorded acceleration except for the period interval of 0 to 0.5 s where the opposite situation prevails. None of the numeric computations were able to reproduce the high peak observed in the spectral curve of the recorded motion at a period of 2.5 s. However it was possible to adjust the soil parameters in such way as to reproduce the spectral curve for period larger than 0.5 s but not without losing the good agreement between the computed and recorded motions for the other horizontal component (210°), Figure 6. The difficulty in finding a set of soil parameters that simultaneously generates a good fit for both components simultaneously suggests the presence of an anisotropic effect in the soil.



D The RIN site

For this site, we were not able to find a set of parameters for which the synthetics and the recorded acceleration time histories were in good agreement. The numerical results suggest that pore pressure did not affect significantly the ground shaking observed at the surface. Based on our results other mechanisms are required to provide a viable explanation for the recorded motion at this site (O'Connell, 1999). The geotechnical parameters are summarized in Table 3. The surface waveforms and their respective response spectra are illustrated in Figures 7 and 8.

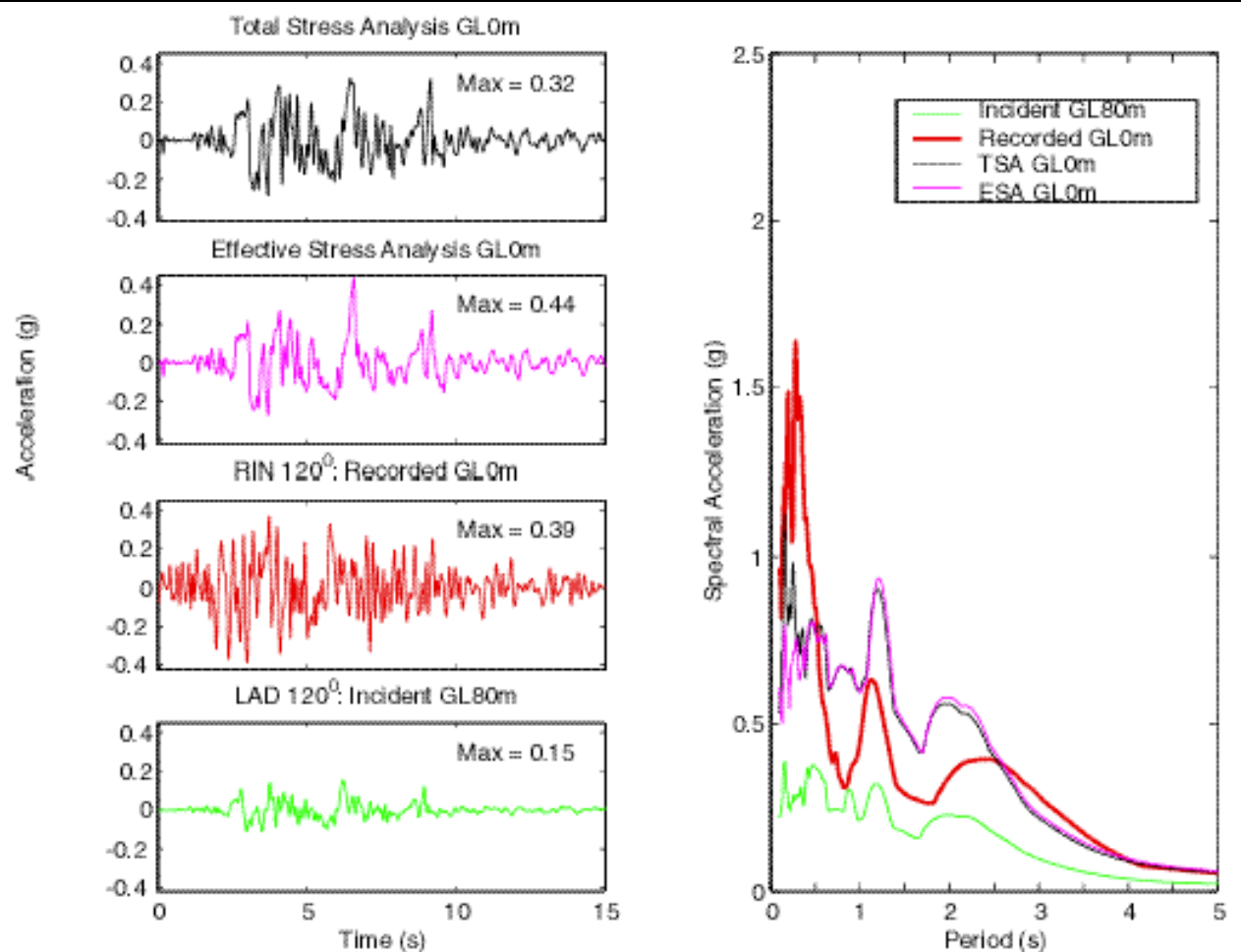


Figure 7: On the left side, the horizontal component (120°) of the computed and recorded acceleration time histories are plotted for the RIN site. The input acceleration time history is shown at the bottom. On the right side are the corresponding 5% damped response spectra. Total stress modeling provide synthetic accelerations (first) in fair agreement with the recorded acceleration (3rd from the top). However, the spectral curves of the computed motions underestimate the high frequencies (period interval of 0 to 0.5 s) in the recorded acceleration. For higher periods (0.5 to 2.5 s) the opposite situation prevails.

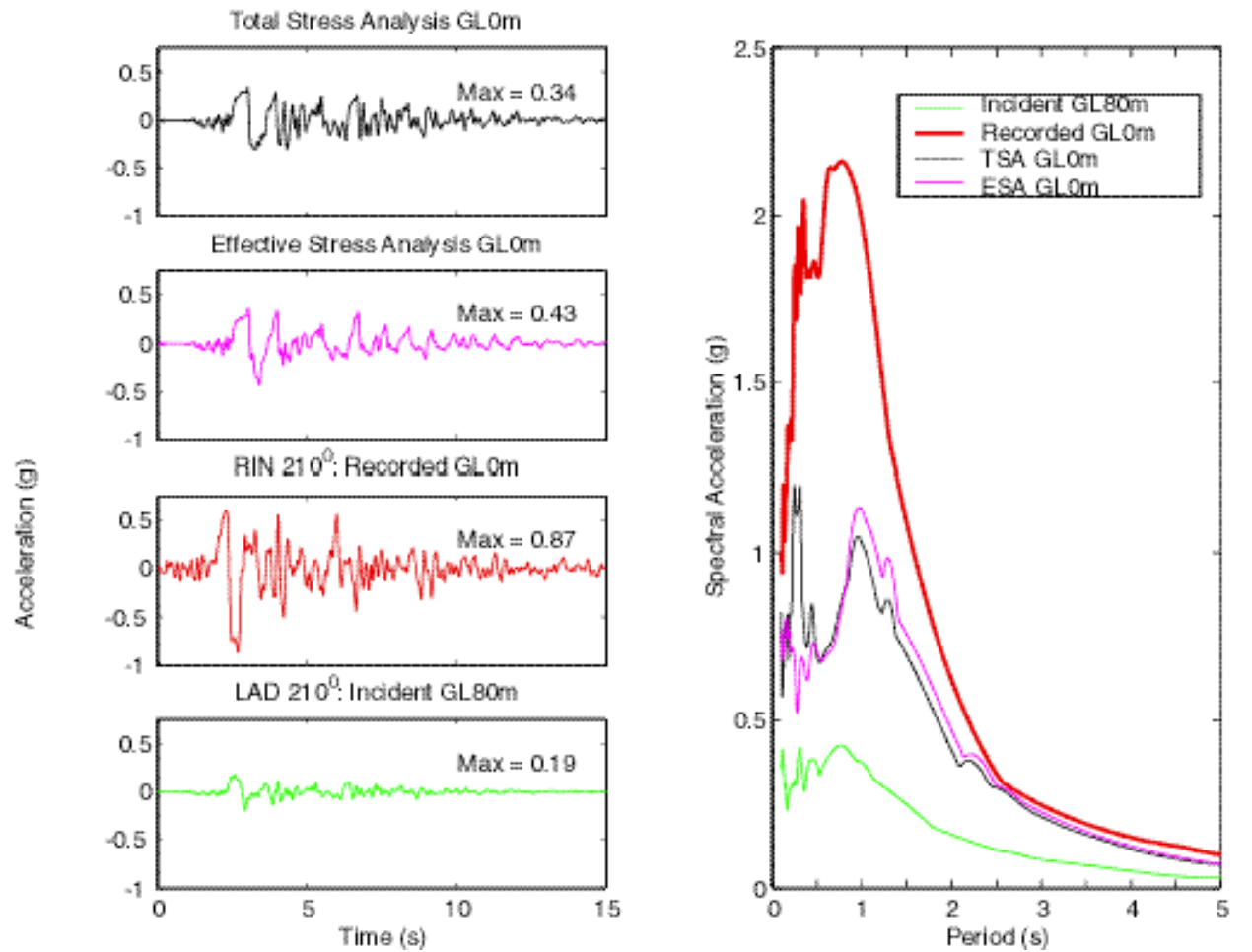


Figure 8: On the left side, the horizontal component (210°) of the computed and recorded acceleration time histories are plotted for the RIN site. The input acceleration time history is shown at the bottom. On the right side are the corresponding 5% damped response spectra. Both synthetic accelerations (first and second left) fail to reproduce the recorded acceleration. Comparison between the spectral curves of the two computed motions and the recorded accelerations confirmed this conclusion. None of our numerical simulations were able to reproduce the large pulse observed in the recorded motion at 3 s. According to Archuleta *et al.* (1998), the amplification of the first S waves is a consequence of the directivity of the rupture for this fault geometry. However both LAD and RIN are within 1.5 km of each other. But even if the incident ground motion (bottom trace) were propagated linearly, it would not be as large as the recorded surface motion (3rd trace from top). Thus including nonlinearity, which generally reduces the amplitude, is not reproducing the surface recording.

Table 3: For all layers, the coefficient of earth at rest is given by $K_0=1.$, the angle of internal friction $\varphi=40^\circ$, the viscosity coefficient $\eta = 5 \times 10^{15}$, and $H_{\max}=30\%$. The layers are numbered from 1 to 8. The water table is located at 10 m depth. The last layer BR, includes the information at the bedrock level. Only layer 4 is capable of pore pressure buildup.

| LAYER NO. | DEPTH (M) | v_s (m/s) | v_p (m/s) | ρ (KG/M ³) | Q | PARAMETERS FOR DILATANCY | | | | | |
|-----------|-----------|-------------|-------------|-----------------------------|-----|--------------------------|-------|-------|-------|-------|-------|
| | | | | | | φ_p | p_1 | p_2 | w_1 | c_1 | S_1 |
| 1 | 4.5 | 172 | 272 | 1800 | 25. | | | | | | |
| 2 | 7. | 294 | 772 | 1800 | 25. | | | | | | |
| 3 | 10 | 294 | 1971 | 1800 | 25. | | | | | | |
| 4 | 12.8 | 294 | 1971 | 1800 | 25. | 30° | .7 | .4 | 2 | 1 | .005 |
| 5 | 21.3 | 466 | 1971 | 1900 | 25. | | | | | | |
| 6 | 40. | 497 | 1971. | 1900 | 25. | | | | | | |
| 7 | 73.3. | 539 | 1971 | 2000 | 25 | | | | | | |
| 8 | 80 | 814 | 1971 | 2200 | 25 | | | | | | |
| BR | | 814. | | 2200 | | | | | | | |

E The SMI site

If we simply deconvolve the surface motion to depth using the measured elastic wave speeds, the synthetic accelerograms systematically underestimate the recorded motions. However if we use the signal recorded at the surface ETEC site (a rock site) as the incident motion for GL-80th, the numerical predictions are closer to the recorded motion especially when pore pressure effects are included. Here the amplitude of the incident signal is considered as an additional free parameter that should be considered to reproduce the motion recorded at the SMI site. The geotechnical parameters are summarized in Table 4. The surface waveforms and their respective response spectra are illustrated in Figures 9 and 10.

Table 4: For all layers, the coefficient of earth at rest is given by $K_0=1.$, the angle of internal friction $\varphi=35^\circ$, the viscosity coefficient $\eta = 5 \times 10^{15}$, and $H_{\max}=30\%$. The layers are numbered from 1 to 9. The water table is located at 6 m depth. The last layer BR, includes the information at the bedrock level. Only layer 3 is capable of pore pressure buildup.

| LAYER NO. | DEPTH (M) | v_s (m/s) | v_p (m/s) | ρ (KG/M ³) | Q | PARAMETERS FOR DILATANCY | | | | | |
|-----------|-----------|-------------|-------------|-----------------------------|-----|--------------------------|-------|-------|-------|-------|-------|
| | | | | | | φ_p | p_1 | p_2 | w_1 | c_1 | S_1 |
| 1 | 2. | 207 | 525 | 1800 | 33. | | | | | | |
| 2 | 6. | 348 | 602 | 1800 | 33. | | | | | | |
| 3 | 7.3 | 348 | 5373 | 1800 | 33. | 24.8° | .4 | .6 | 2. | 1 | .005 |
| 4 | 12.8 | 314 | 5373 | 1800 | 33. | | | | | | |
| 5 | 15 | 1180 | 5373 | 2200 | 33. | | | | | | |
| 6 | 27. | 1180 | 2562 | 2200 | 33. | | | | | | |
| 7 | 33.5. | 1202 | 2562 | 2200 | 33 | | | | | | |
| 8 | 40 | 1497 | 2562 | 2200 | 33 | | | | | | |
| 9 | 80 | 1497 | 3115 | 2300 | 33 | | | | | | |
| BR | | 14497 | | 2300 | | | | | | | |

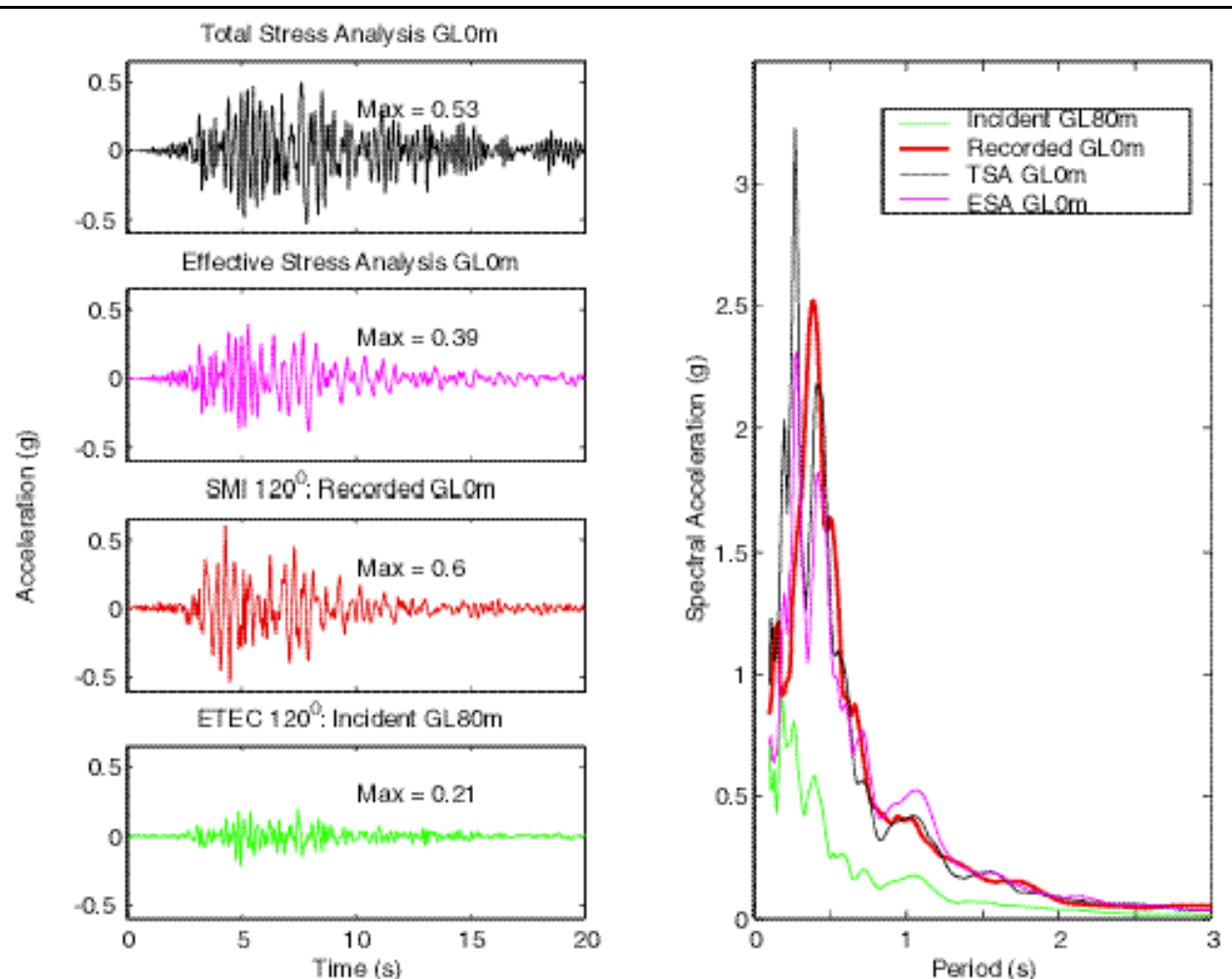


Figure 9: On the left side, the horizontal component (120°) of the computed and recorded acceleration time histories are plotted for the SMI site. The input acceleration time history is shown at the bottom. On the right side are the corresponding 5% damped response spectra. Inclusion of pore pressure into the nonlinear model provides a synthetic acceleration (2nd from the top) in good agreement with the recorded acceleration (3rd from the top) over the entire time interval except for a short time interval between 3 and 5 s. Note the depletion of the high frequency in the synthetic signal in good agreement with the recorded acceleration. The spectral curve of the effective stress method is in good agreement with the data for the entire frequency range except for the interval of 0 to 0.5 s.

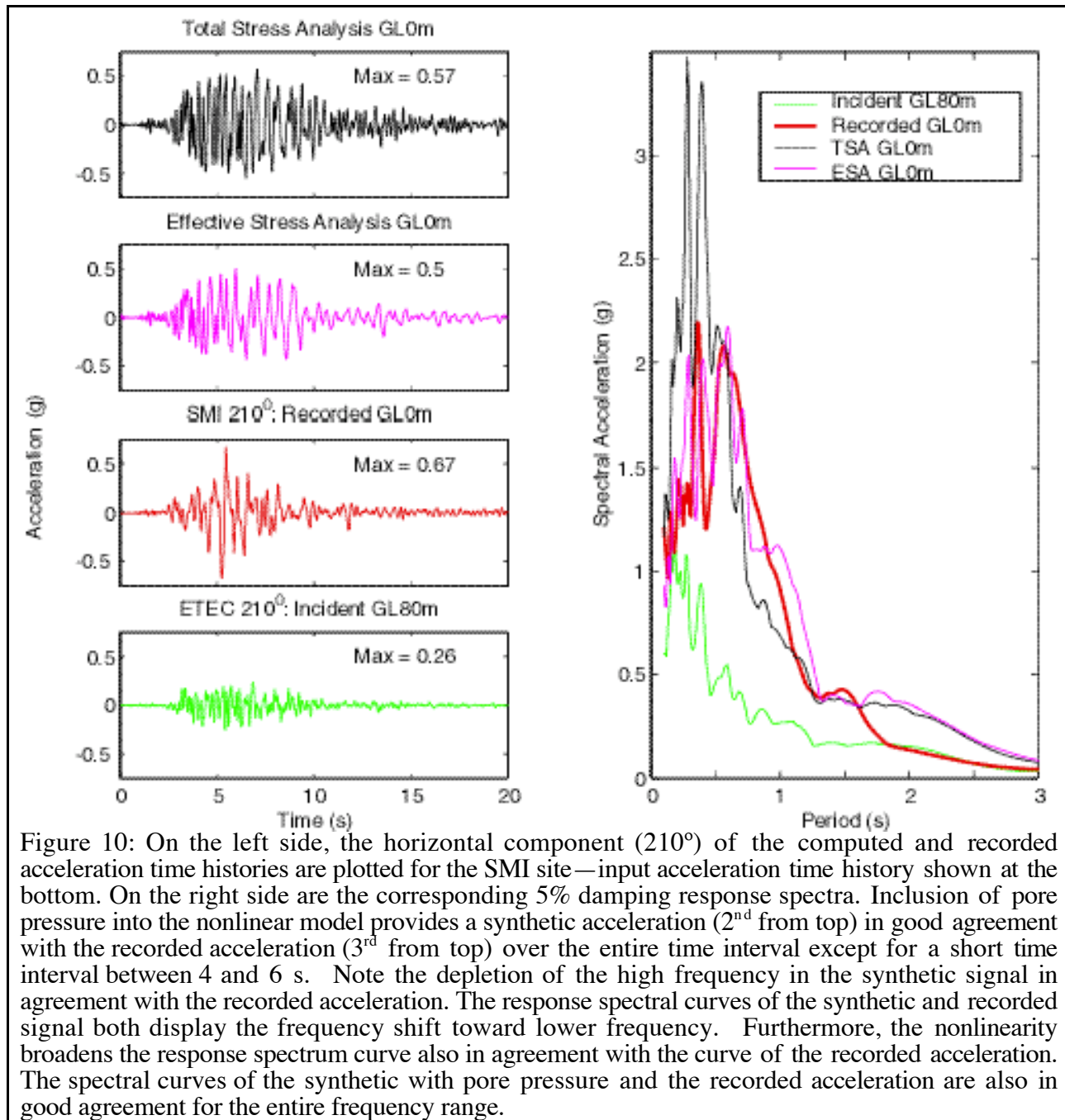


Figure 10: On the left side, the horizontal component (210°) of the computed and recorded acceleration time histories are plotted for the SMI site—input acceleration time history shown at the bottom. On the right side are the corresponding 5% damping response spectra. Inclusion of pore pressure into the nonlinear model provides a synthetic acceleration (2^{nd} from top) in good agreement with the recorded acceleration (3^{rd} from top) over the entire time interval except for a short time interval between 4 and 6 s. Note the depletion of the high frequency in the synthetic signal in agreement with the recorded acceleration. The response spectral curves of the synthetic and recorded signal both display the frequency shift toward lower frequency. Furthermore, the nonlinearity broadens the response spectrum curve also in agreement with the curve of the recorded acceleration. The spectral curves of the synthetic with pore pressure and the recorded acceleration are also in good agreement for the entire frequency range.

5 REFERENCES

- Archuleta, R. J. Direct observation on nonlinearity in accelerograms *Proceeding of the Second International Symposium on the Effects of Surface Geology on Seismic Motion*, **Vol. 2**, edited by K. Irikura, K. Kudo H. Okada and T. Sasatani, A.A. Balkema: Netherlands. 787-792, 1998.
- Archuleta, R. J., P. Liu, J. H. Steidl, L. F. Bonilla, D. Lavallée, and F. Heuze, 2002. Finite-Fault Site-Specific Acceleration Time Histories That Include Nonlinear Soil Response. *Physics of the Earth and Planetary Interiors*.

- Archuleta, R.J., L. F., Bonilla, and D. Lavallée. *Proceeding of the 12th World Conference on Earthquake Engineering*, published by Aston Koedyk Ltd. Paper reference number 0338, 2000.
- Archuleta, R.J., L.F. Bonilla, and D. Lavallée. *Proceedings of the OECD-NRC Workshop on Engineering Characterization of Seismic Input*, Brookhaven National Laboratory, NY, 32 pp, 1999.
- Archuleta, R. J., G. Mullendore and L. F. Bonilla. Separating the variability of ground motion over small distance. *Proceeding of the Second International Symposium on the Effects of Surface Geology on Seismic Motion*, **Vol. 2**, 1059-1065, 1998.
- Bardet, J. P., F. Oka, M. Sugito and A. Yashima. The Great hanshin earthquake disaster, Prelim. Invest. Rep., University of Southern California, Los Angeles, CA. 1995.
- Bonilla, L. F., D. Lavallée, and R. J. Archuleta. *Proceeding of the Second International Symposium on the Effects of Surface Geology on Seismic Motion*, **Vol. 2**, edited by K. Irikura, K. Kudo H. Okada and T. Sasatani, A.A. Balkema: Netherlands, 793-800, 1998.
- Bonilla, L. F. Computation of Linear and Nonlinear Site Response for Near Field Ground Motion, Ph.D. dissertation, University of California, Santa Barbara, 285 pp, 2000.
- Cultrera, G., D. M. Boore, W. B. Joyner, and C. M. Dietel. Evidence for nonlinear soil response at the Van Norman Complex, CA, USA, following the 1994 Northridge earthquake. *Proceeding of the Second International Symposium on the Effects of Surface Geology on Seismic Motion*, **Vol. 2**, 779-786, 1998.
- Field, H. E., P. A. Johnson, I. A. Beresnev and Y. Zeng, Nonlinear ground-motion amplification by sediments during the 1994 Northridge earthquake, *Nature*, **390**, 599-602, 1997.
- Gibbs, J. F., J. C. Tinsley, and W. B. Joyner. Seismic velocities and geological conditions at twelve sites subjected to strong ground motion in the 1994 Northridge, California, earthquake. *U.S. Geological survey Open-File Report 96-740*, 1996.
- Gibbs, J. F., J. C. Tinsley, D. M. Boore, and W. B. Joyner. Seismic velocities and geological conditions at twelve sites subjected to strong ground motion in the 1994 Northridge, California, earthquake: A revision of OFR 96-740. *U.S. Geological survey Open-File Report 99-446*, 1999.
- Gibbs, J. F., J. C. Tinsley, D. M. Boore, and W. B. Joyner. Borehole velocity measurements and geological conditions at thirteen sites in the Los Angeles, California region. *U.S. Geological survey Open-File Report 00-470*, 2000.
- Iai, S., Y. Matsunaga and T. Kamoka. *Report of Port and Harbour Research Institute*, **29**, No 4, 27-55, 1990a.
- Iai, S., Y. Matsunaga and T. Kamoka. *Report of Port and Harbour Research Institute*, **29**, No 4, 57-83, 1990b.
- Ishihara, K. stability of natural deposit during earthquake. *Proc. 11th Int. Conf. On Soil Mechanics and Foundation Engineering*, San Francisco, 327-376, 1985.
- Joyner, W. B. A. T. F. and Chen, Calculation of nonlinear ground response in earthquakes, *Bull. Seism. Soc. Am.*, **65**, 1315-1336, 1975.
- Kramer, S. L. *Geotechnical Earthquake Engineering*, Prentice Hall, New Jersey, 1996.
- Lavallée, D., L.F. Bonilla, and R. J. Archuleta. Hysteresis model for nonlinear soil under Irregular cyclic loadings: Introducing the Generalized Masing Rules. Submitted to *Journal of Geotechnical and Geoenvironmental Engineering*.
- Li and Liao, Dynamic skeleton curve of soil stress-strain relation under irregular cyclic loading, *Earthquake research in China*, **7**, 469-477, 1993.
- Mozco, P. Introduction to Modeling Seismic Wave Propagation by the Finite Difference Method. Lecture note given at the Disaster Prevention Research Institute, Kyoto University, 1998.
- O'Connell, D. R. H., Replication of apparent nonlinear seismic response with linear wave propagation models, *Science* **283**, 2045-2033, 1999.
- Pyke, R. Nonlinear soil model for irregular cyclic loadings. *J. of the Geotech. Eng. Div.* **105** (6), 715-726, 1979.
- Seed, H. B. Landslide during earthquake due to soil liquefaction, *J. of Soil Mechanics and Foundations Divisions*, ASCE, **94**, 1053-1122, 1966.

Towhata, I. and K. Ishihara. *Fifth International Conference on Numerical Methods in Geomechanics*, Nagoya, 523-530, 1985.

REPORTS PUBLISHED

No report resulting from this work has been published.